

Direct-Laser-Written Polymer Nanowire Waveguides for Broadband Single Photon Collection from Epitaxial Quantum Dots into a Gaussian-like Mode

Edgar F. Perez,* Cori Haws, Marcelo Davanco, Jindong Song, Luca Sapienza, and Kartik Srinivasan*

Single epitaxial quantum dots (QDs) embedded in nanophotonic geometries are a leading technology for quantum light generation. However, efficiently coupling their emission into a single mode fiber or Gaussian beam often remains challenging. Here, direct laser writing (DLW) is used to address this challenge by fabricating 1 μm diameter polymer nanowires (PNWs) in-contact-with and perpendicular-to a QD-containing GaAs layer. QD emission is coupled to the PNW's HE_{11} waveguide mode, enhancing collection efficiency into a single-mode fiber. PNW fabrication does not alter the QD device layer, making PNWs well-suited for augmenting pre-existing in-plane geometries. Standalone PNWs and PNWs in conjunction with metallic nanoring devices that have been previously established for increasing extraction of QD emission are studied. Methods that mitigate standing wave reflections and heat, caused by GaAs's absorption/reflection of the lithography beam, and which otherwise prevent PNW fabrication, are also reported. A maximum improvement of $(3.0 \pm 0.7)\times$ in a nanoring system with a PNW compared to the same system without a PNW is observed, in line with numerical results, and highlighting the PNW's ability to waveguide QD emission and increase collection efficiency simultaneously. These results demonstrate new DLW functionality in service of quantum emitter photonics that maintains compatibility with existing top-down fabrication approaches.

1. Introduction

As fundamental building blocks, single photons (SPs) and entangled photons play key roles in the development of quantum science,^[1,2] and their efficient generation and collection into optical fibers is crucial for quantum technologies such as quantum simulation and quantum communication.^[3,4] Among many options, semiconductor quantum dots (QDs) are a promising source of single photons, with recent demonstrations approaching the technical readiness level required by various applications.^[5–8] The success of the platform is largely supported by top-down fabrication techniques that enable the implementation of photonic structures that host the QDs and enhance their performance. However, in many such photonic geometries, realizing high fiber-coupled collection efficiency of SP emission remains an important challenge that, if unaddressed, limits the SP flux delivered to many downstream applications. A viable solution to this problem should ideally increase the collection efficiency without

compromising other important performance characteristics, such as SP purity and indistinguishability. To that end, several different efforts to realize such solutions are underway.^[9–11]

In recent years, Direct Laser Writing (DLW) has been used to create a variety of 3D structures that improve fiber-to-chip coupling^[12–14] with increasing levels of automation,^[15,16] and complexity.^[17] In the context of SP emission, direct laser written solutions for epitaxially-grown, semiconductor QDs have focused on the fabrication of micro-optics^[14,18–20] that shape and collect their far-field radiation. A variety of DLW structures have also been used for collection efficiency enhancement from other single quantum emitters, such as color centers in diamond nanocrystals^[21] and organic molecules.^[22] In this work, we use DLW to fabricate high-index-contrast cylindrical waveguides, hereafter referred to as polymer nanowires (PNWs), perpendicular to the surface of a semiconductor-based SP emitter substrate. The PNWs operate on the near-field radiation of a SP emitter to directly waveguide-couple its emission to an HE_{11} optical mode that can be well-coupled to a downstream optical fiber.

E. F. Perez, K. Srinivasan
Joint Quantum Institute
NIST/University of Maryland
College Park 20742, USA
E-mail: perezed@umd.edu; kartik.srinivasan@nist.gov

E. F. Perez, M. Davanco, K. Srinivasan
Microsystems and Nanotechnology Division
National Institute of Standards and Technology
Gaithersburg 20899, USA

C. Haws, L. Sapienza
Nanoscience Centre, Department of Engineering
University of Cambridge
Cambridge CB3 0FA, United Kingdom

J. Song
Center for Opto-Electronic Materials and Devices Research
Korea Institute of Science and Technology
Seoul, South Korea

 The ORCID identification number(s) for the author(s) of this article can be found under <https://doi.org/10.1002/qute.202300149>

DOI: 10.1002/qute.202300149

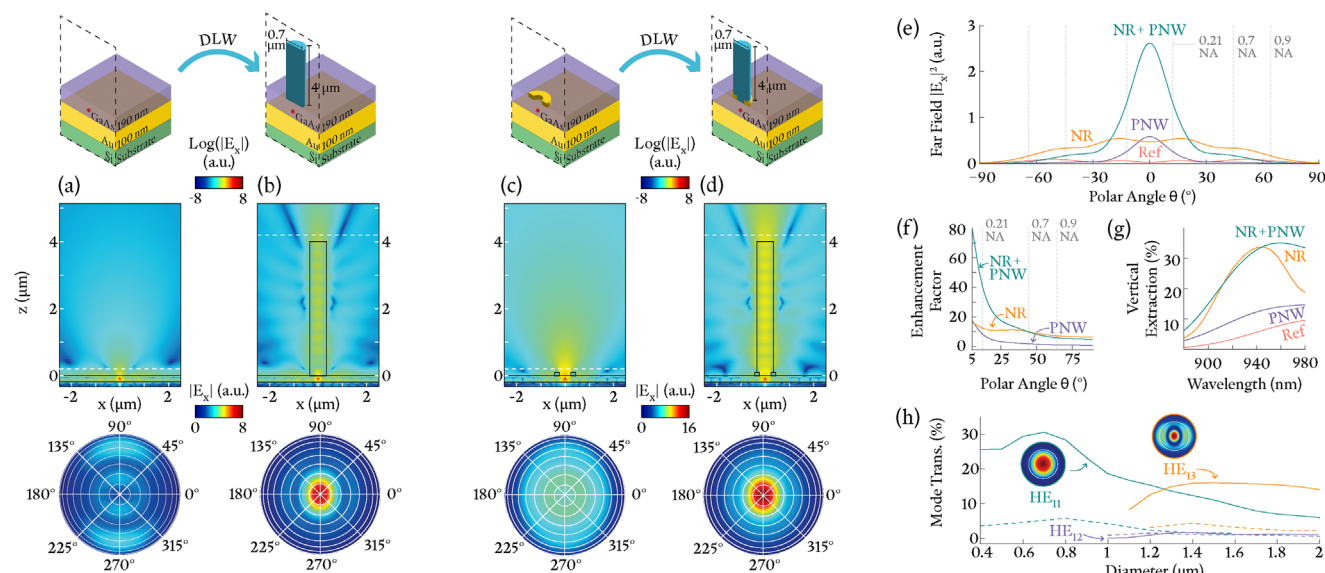


Figure 1. a–d) 3D FDTD simulations of systems with and without polymer nanowires (PNWs). For each system (a–d), the top panel is a schematic of the physical device, the middle panel is a cross-section of the system’s 3D FDTD simulation, and the bottom panel is the far-field projection of the system’s emission. The black dashed rectangles in the top panel frame the cross-sectional planes displayed in the middle panels, and the white lines in the middle panels indicate the height at which the emission was sampled for the far-field projections shown in the bottom panels. a) A reference system, consisting of an x-polarized dipole in the middle of a 190 nm thick GaAs layer on top of a 100 nm-thick Au back reflector, taken as a starting point for systems in (b, d). b) A standalone PNW system, with a 0.7 μm diameter PNW of 4 μm length, centered over the dipole, showing emission confined- and guided-by the PNW waveguide. c) A metallic nanoring (NR) system, consisting of an Au NR of inner diameter 236 nm, outer diameter of 437 nm, and 100 nm thickness centered above the QD. d) A metallic NR system with the same dimensions as in (c) and a concentric 0.7 μm diameter PNW of 4 μm length (i.e., the NR+PNW system). e) Line scans ($\phi = 90^\circ$, y-axis) of the $|E_x|^2$ far-field projections for each system. The PNW (purple) and NR+PNW (green) systems have monotonic and Gaussian-like distributions, whereas the reference (pink) and NR (orange) systems without PNWs have wide and nonmonotonic distributions. f) The ratio of $|E_x|^2$ intensity emitted by the PNW (purple), the NR (orange), and the NR+PNW (green) systems compared to the reference system, as a function of polar angle θ . See text for details. g) The transmission of each system through a plane 200 nm above the substrate, showing that all four schemes are broadband. h) Transmission into the various optical modes of the PNW system (dashed) and the PNW+NR system (solid) as a function of PNW diameter. Insets display the $|E_x|$ component of the HE_{11} mode (green) and HE_{13} mode (orange) of a PNW with 1.3 μm diameter (circumference shown as white line). The HE_{12} mode (purple) of the system is only weakly excited due to poor overlap with an x-polarized dipole. The white dashed horizontal lines are located 200 nm above the substrate in panels (a) and (c) and 200 nm above the PNWs in panels (b) and (d). See Supporting Information for more details.

Additionally, the fabrication of PNWs does not require etching of the underlying QD-hosting material, which has two important implications. First of all, it mitigates negative effects that can arise when emitters are located in the vicinity of sidewalls.^[23] Second, PNWs can be fabricated in conjunction with existing on-chip solutions like other broadband collection-enhancing devices or etched resonant cavities.

In this work, PNWs are studied as standalone devices and in conjunction with metallic nanorings (NRs), which are broadband collection-enhancing devices,^[24–26] to improve the collection efficiency from epitaxially grown InAs/GaAs QDs. PNWs prove to be effective at waveguide-coupling the emission from QDs and we observe a factor of $(3.0 \pm 0.7) \times$ improvement in collection efficiency in a NR system with a PNW compared to the same system without a PNW. The inherently broadband nature of waveguide collection, together with the low dispersion of polymers commonly used in DLW,^[27] results in improvements in collection efficiency over a large bandwidth. Moreover, the collection into an HE_{11} optical mode is advantageous for direct fiber-coupling applications.

Section 2.1 contains a numerical investigation comparing systems with and without PNWs, including the effect of PNW geom-

etry, and the excitation of the various modes of the PNW waveguide. Two key challenges to the fabrication of these devices are standing wave reflections and heating; we present DLW strategies that mitigate these problems in Section 2.2. Optical characterization of the fabricated PNWs is presented in Section 2.3, and we conclude by commenting on the utility that PNWs bring to integrated quantum light sources. PNWs extend the role DLW plays in SP collection by working with near-field emission to directly waveguide-couple SP radiation and increase collection efficiency.

2. Results and Discussion

2.1. Polymer Nanowire Design

Polymer nanowires are shown as stand alone devices in Figure 1a,b, and as complementary devices in Figure 1c,d. For each system, Figure 1a–d provides a schematic of the device (top), a cross-section of 3D finite-difference time-domain (FDTD) simulations of the system (middle), and far-field projections of each system’s emission (bottom). The dashed black rectangle in the top panels indicates the cross-sectional plane displayed in the middle panels. Likewise, the dashed white line in each middle

panel indicates the distance from the GaAs substrate at which the emission was sampled for the far-field projections. The device illustrated in Figure 1a consists of an x-polarized dipole source (emission wavelengths from 880 to 980 nm) embedded in the middle of a 190 nm layer of GaAs with an Au back reflector. This system has been used in recent studies for broadband collection enhancement,^[24,28,29] and this work takes it as a reference point for understanding the improvements offered by PNWs.

The fundamental concepts of PNW-guided emission can be understood by comparing the reference system in Figure 1a to the standalone PNW system in Figure 1b. The reference system shows in-plane dipole emission that is significantly trapped in the GaAs layer, with the limited free-space emission quickly diverging. The $|E_x|$ component of the far-field projection of the system's emission shows a local minimum at its center and strong radiation at polar angles greater than 40° , which is not well suited for coupling to the LP_{01} (fundamental, linearly polarized) mode of a single-mode fiber. In contrast, simulating a 4 μm tall PNW with a 700 nm diameter concentric to the dipole, as shown in Figure 1b, illustrates that the PNW laterally confines radiation as it propagates through the PNW, along the z-axis, with a far-field distribution that resembles the LP_{01} mode of a fiber. Line scans along the $\phi = 90^\circ$ axis (i.e., the y-axis) of the $|E_x|^2$ far-field distributions are directly compared in Figure 1e, which verifies that the distribution of the standalone PNW system (purple) is more Gaussian-like, with a single maximum of greater amplitude at its center, compared to the reference system (pink).

The use of a PNW as a complementary device is studied in Figure 1c,d, where it is simulated above a metallic NR. As previously reported,^[24–26,30] the NR system shown in Figure 1c shows an increase in vertical radiation compared to the reference system, yet displays a local minimum at its center and a large divergence angle. When the NR system is complemented with a PNW (referred to as the NR+PNW system) the emission from the NR is coupled to the optical modes of the PNW. As shown in Figure 1d,e, this results in a far-field projection with a single maximum at its center that is of greater amplitude than that of the NR system alone. As a complementary device, the PNW has shifted the far-field $|E_x|^2$ distribution toward smaller angles by coupling it to the HE_{11} mode of the PNW.

For each of the PNW, NR, and NR+PNW systems, Figure 1f plots the ratio of the integrated electric field intensity within a solid polar angle θ , calculated as $\int |E_x|^2 d\Omega$, in the system to that of the reference system. As expected, the PNW system (purple) and the NR+PNW system (green) increase the radiation at small angles. At large angles, the total extracted power of the PNW systems approaches the total extracted power of the underlying system, suggesting that the PNWs have limited effect on the extraction efficiency of the underlying devices. In other words, the PNWs operate on the near field emission of the QD systems to increase collection efficiency without significant modification to their performance. For $\theta \approx 12^\circ$, the divergence angle of SM980 fiber,^[31] the PNW (NR+PNW) system shows an increase of approximately $8.5\times$ ($41.0\times$) in collection efficiency compared to the reference system. For the same angle, the NR+PNW system shows approximately $3.3\times$ the collection efficiency of the NR system without a PNW (orange curve). Finally, Figure 1g compares the broadband performance of each system and shows that PNWs (purple) are broadband devices, making them compati-

ble with NR systems (orange), endowing the NR+PNW system (green) with broadband performance as well.

Like most waveguides, the optical properties of a PNW will depend on its geometry. Figure 1h shows the simulated transmission of dipole radiation into various optical modes of the PNW as a function of nanowire diameter D for the standalone system (dashed) and the NR+PNW system (solid). In general, the two systems display similar behavior, with the collection from the NR+PNW system being approximately $4\times$ to $6\times$ greater. As expected, there is an optimal diameter $D \approx 700$ nm at which coupling into the fundamental HE_{11} mode of the PNW is maximized. At the optimal diameter, $\approx 30.5\%$ of the total power emitted by the dipole is coupled to the HE_{11} optical mode of the PNW, with a monotonic decrease for $D > 700$ nm. The initial decrease (i.e., for $700 \text{ nm} < D < 1 \mu\text{m}$) is not associated with the excitation of higher order modes, so it is attributed to a mismatch in the PNW mode profile and the emission of the underlying device, meaning that it may be possible to design a PNW in conjunction with underlying devices to prevent this decrease. When $D \approx 1.3 \mu\text{m}$, coupling to the HE_{13} mode of the PNW begins to dominate and coupling to the HE_{11} mode is reduced by half. We note that coupling to the HE_{12} mode of the PNW is inefficient at all diameters due to poor overlap with an x-polarized dipole.

In summary, numerical studies of PNWs support their use as interfaces for direct waveguide-coupling of dipole emission from solid-state SP emitters. In both standalone and cooperative systems the PNWs offer waveguiding, HE_{11} emission profiles, and significant far-field enhancement for small emission angles $\theta \lesssim 20^\circ$. QD emission couples to the fundamental mode of PNWs for $D \leq 1 \mu\text{m}$, with an ideal diameter of 700 nm. However, beyond 700 nm, the large degree of overlap between the HE_{11} mode of the PNW and the LP_{01} mode of a single-mode fiber, together with the small divergence of PNW emission, may still provide an overall increase in the fiber collection efficiency of a system.

2.2. Fabrication of PNWs

The direct laser writing used in this study employs strongly focused 780 nm femtosecond laser pulses to polymerize a small voxel of photoresist through two photon excitation. Despite the minimum resolution of DLW systems routinely reaching sub-micron scales,^[32–34] the DLW of sub-micron features requires special attention to proximity effects during exposure^[35] and structural deformations during development.^[36] Near the surface of reflective and absorptive substrates like GaAs, additional challenges arise. The partial reflection of the high intensity lithography pulses induces standing waves that lead to modulations of the effective exposure dose. Furthermore, the partial absorption of the pulses causes local heating of the substrate, resist, and any underlying structures, which affects the polymerization threshold of the resist.^[37] Each of these effects deteriorates the quality of small features near a substrate, and realizing sub-micron diameter PNWs requires their mitigation.

A standard approach to DLW may use a flat substrate, uniform laser power, and a solid-core design in the fabrication of PNWs, like that illustrated in Figure 2a. Fabrication outcomes from the use of this scheme with IP-Dip photoresist^[31] are shown in Figure 2b,i–iii, where unmitigated reflections cause deep

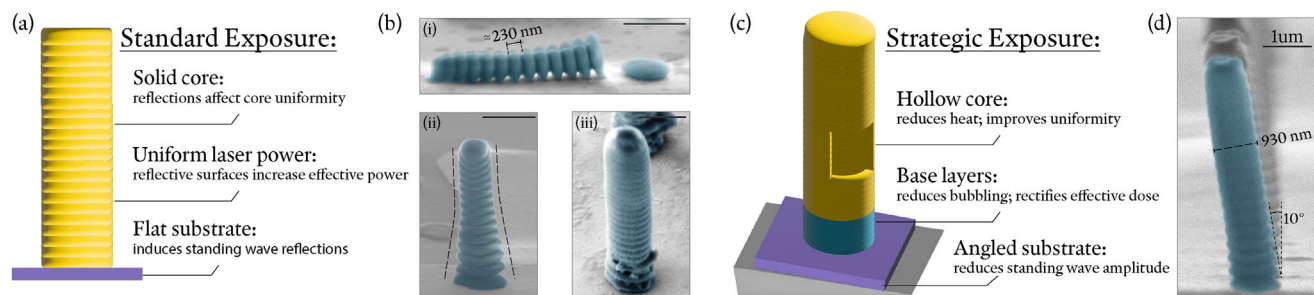


Figure 2. a) A standard approach to DLW structures may use a flat substrate, uniform laser power, and a solid-core design. b,i) False-color SEM images showing a modulation in the PNW diameter with periodicity of ≈ 230 nm due to standing wave reflections of the pulsed 780 nm lithography beam. b, ii) Reflections from the substrate also cause a local increase in the effective laser power near the substrate, which increases the diameter of the PNW near the surface. b,iii) Absorption of the lithography beam further contributes to local heating of resist, which can lead to deformations and resist vaporization (e.g., “bubbling”). c) The exposure strategy used in this work with a substrate mounted at a 10° angle, reduced-power base layers, and a hollow core. d) False-color SEM images showing PNWs with improved uniformity and decreased corrugation amplitudes realized with the proposed exposure strategy. The 3D flexibility of DLW is used to correct for the angle induced by the angled substrate in (d) (see Figure 3), but is intentionally included in this device for illustrative purposes. All scale bars correspond to $1\ \mu\text{m}$.

standing-wave-induced corrugations that can separate PNWs at their base (i), an increase in the diameter of the PNW near its base (ii) (due to increased effective dose), and a shift of the polymerization/damage thresholds that can cause vaporization of the resist (e.g., “bubbling”) near the substrate (iii). As shown in Figure 2b,i the period of the corrugations are approximately 230 nm, which roughly correlates with the expected period of 253 nm for normally-incident plane waves from a 780 nm continuous wave laser in IP-Dip.

To mitigate heat generation and reflections, we employed the exposure strategy shown in Figure 2c. In this strategy, a custom mount positions the GaAs substrate at a 10° angle relative to the lithography beam to limit the overlap between incident and reflected pulses; base layers of lower lithography power rectify variations in effective dose; and a hollow-core design reduces local heating by limiting the total dose required to fabricate the PNW. After exposure, samples were UV-cured in a solvent bath to polymerize their cores and prevent structural deformation.^[36] The scanning electron micrograph (SEM) shown in Figure 2d demonstrates the successful fabrication of a PNW at the 10° angle provided by the custom mount. In all subsequent fabrication runs, a -10° correction was applied to the PNW design to compensate for the $+10^\circ$ angle introduced by the mount, which is possible due to the 3D flexibility of DLW. The angled PNW shows greatly reduced corrugation amplitudes and improved uniformity compared to those in Figure 2b.

To validate the general exposure strategy proposed in Figure 2c, a total of 120 PNWs of varying diameters were fabricated on the reference substrate shown in Figure 1a. The nanowires were fabricated using IP-Dip photoresist,^[31] 6.25 to 12 mW of time-averaged laser power, with 80 to 100 fs pulses focused by a numerical aperture (NA) 1.4 objective at an 80 MHz repetition rate and a laser scan speed of $1\ \text{mm}\ \text{s}^{-1}$. As shown in Figure 3a,b, the fabrication had a 100 percent yield of angle-corrected (i.e., straight-standing and perpendicular to the substrate) PNWs with reduced corrugation depths. Figure 3c shows PNWs with diameters varying from 0.9 to $1.8\ \mu\text{m}$, showing the uniformity of each design with respect to diameter. Assuming a fixed and finite width for the PNW’s cylindrical walls, as the outer diameter decreases, so too must the hollow void in the PNW.

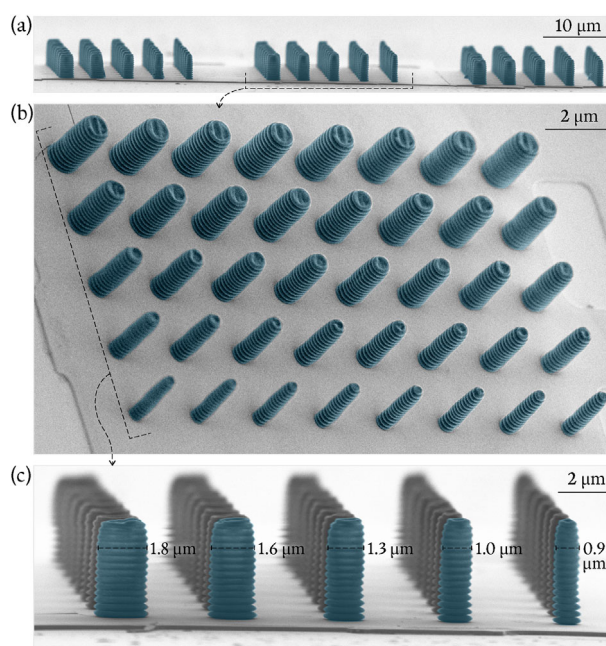


Figure 3. a) False-color SEM images of PNWs fabricated on GaAs substrates with Au back reflectors with 100 % yield using the strategy proposed in Figure 2c. b) A perspective view of the central set of devices in (a), showing straight-standing PNWs of different diameters. c) A lateral view of a PNW array, showing greatly reduced sidewall corrugations at all diameters compared to those fabricated using a standard strategy (Figure 2b).

Thus, at small diameters, the PNW may not be completely or uniformly hollow, but the use of a hollow design prevents rasterization and heat accumulation in the inner volume. Despite the Au back reflector in the reference design providing very strong reflections, the angled substrate reduced the depth of the corrugations to ≈ 150 nm for the reference system and ≈ 50 nm for PNWs printed on GaAs with no back reflector (Figure 2d).

Despite the progress on PNW fabrication, the persistence of the corrugations warrants a numerical understanding of their influence on device performance. Figure 4a shows the fabrication

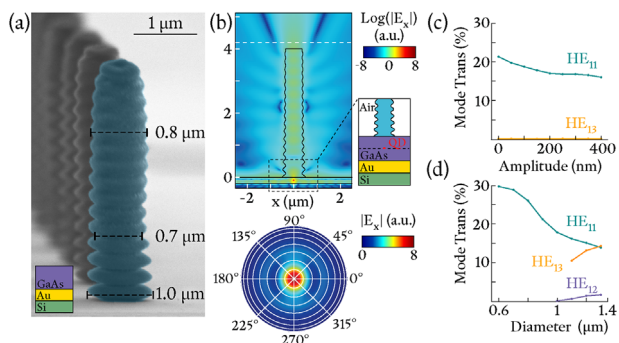


Figure 4. a) Close up scanning electron micrograph of a PNW on a GaAs substrate with an Au back reflector and showing an ≈ 150 nm corrugation amplitude. b) FDTD simulation of a corrugated PNW showing that light is still confined in a PNW mode propagating along the z -axis (top) and far-field emission is still azimuthally symmetric and Gaussian-like. c) The coupling efficiency into the HE_{11} modes of a $1 \mu\text{m}$ diameter PNW as a function of corrugation amplitude. d) The excitation of higher order modes for a fixed corrugation amplitude but varying PNW diameter, showing similar performance to the uncorrugated device in Figure 1h.

of a PNW on the reference substrate (inset) with various dimensions highlighted to show diameter variation along the z -axis. In particular, the device shows corrugation amplitudes that decrease as a function of the distance z from the substrate surface. Corrugations were introduced into FDTD simulations as a variation of the diameter $D(z) = D_0 + \delta(z)$ with $\delta(z) = \frac{2A}{1+\gamma z} \cos^2(z \frac{\pi}{\lambda_c})$, where A is the corrugation amplitude, γ linearly decreases the amplitude for increasing z , and λ_c is the corrugation wavelength. Figure 4b shows an FDTD simulation for a PNW on the reference substrate with $D_0 = 0.7 \mu\text{m}$, $A = 150$ nm, $\gamma = 0.75$, and $\lambda_c = 230$ nm. As shown in the simulation, the corrugated device still confines emission to the z -axis and has a Gaussian-like far-field distribution amenable to fiber-coupling. The effect of the corrugation amplitude is investigated in Figure 4c, which shows that the corrugation depth monotonically reduces the coupling efficiency from the dipole to the HE_{11} mode of the PNW. Even so, for $A = 200$ nm the corrugations introduce $< 20\%$ loss compared to the ideal PNW with $A = 0$ nm. The modulations tend to shift the average diameter of the PNW, so that a small shift in the optimal waveguide dimensions is expected. Fixing the corrugation depth to 150 nm depth, like that of the fabricated device in Figure 4a, and varying D_0 (Figure 4d) verifies that the optimal diameter decreases to ≈ 600 nm. In general, the corrugations reduce the optimal PNW diameter and the HE_{11} mode transmission, but they do not prevent the PNW from confining radiation and emitting a directional gaussian-like mode.

2.3. Optical Characterization of PNWs

Implementing the fabrication strategy proposed above, PNWs were fabricated on both the reference structure (shown in Figure 3) and on the NR devices, as shown in Figure 5c. To avoid spurious reflections from the Au NR, the PNWs fabricated on NRs had $D_0 \approx 1.4 \mu\text{m}$, which reduces the PNW-to-NR coupling efficiency, as shown in Figure 4d, but provides an emission profile that overlaps well with the LP_{01} mode of a single mode fiber.

The standalone PNW and the NR+PNW systems were optically characterized using the micro-photoluminescence set up shown in Figure 5a. The devices were cooled to a temperature of ≈ 4 K in a closed-loop cryostat, and illuminated using a 980 nm light emitting diode (LED) or a 780 nm tunable laser. The laser was operated with continuous-wave emission for above-band QD excitation and the LED provided broadband wide-field illumination of the substrate. The laser source is focused onto the sample by a 0.7 NA objective to a spot approximately $1.4 \mu\text{m}$ in diameter. On the other hand, the LED source is collimated on the sample to provide wide-field illumination. During data acquisition, only the excitation beam was active, i.e., the wide-field LED illumination was turned off. The focal plane of the objective is at the top of PNWs (NRs) for measurements of PNW (NR) emission, and the collected signal is routed to an electron multiplying charge-coupled device (EMCCD) camera and a 0.5 m long grating spectrometer through a series of beamsplitters with splitting ratios and positions as indicated in Figure 5a. We note that the spectrometer measures QD emission as collected by a SM980 single mode fiber.

Figure 5b shows a representative image captured by the EMCCD when a PNW array is illuminated by the LED and the laser simultaneously. The objective is focused on the top plane of a PNW array, and each PNW appears as a small darkened dot in the image. Using a piezo stage within the cryostat, the excitation can be aligned to a PNW, the result of which is shown in the left panel of the figure. In this image, the laser appears as a bright illuminated circle. On the other hand, displacing the excitation beam in a lateral direction produces the image shown in the right panel, where the excitation beam is not confined by the PNW, thus diverging to a large out-of-focus spot spread out on the substrate surface. These images demonstrate that the PNWs are functioning as waveguides perpendicular to the substrate surface.

In order to quantify the impact of PNWs on a QD's emission, the same QD should be measured before and after the fabrication of a PNW. The metallic NR platform is well suited for this comparison given that the centers of the rings provide a well-defined location for optical measurements before and after PNW fabrication. We note that the NR broadband enhancement is not detrimental to single-photon purity levels and that lifetimes are not modified by these devices.^[26] Figure 5c shows a set of six PNWs printed directly on an array of metallic NRs, which were fabricated on a GaAs substrate with a high density of emitters. More than 100 QDs were studied before and after PNW fabrication, and the PNW highlighted by the green arrow, which is centered over a NR, is representative of the best performance achieved (the performance varies between devices due to the lack of control of the spatial location of the QDs with respect to the NR and PNW). Figure 5d shows the emission spectra of this NR before (orange) and after (green) the fabrication of the PNW. The top and bottom axes of this figure correspond to the emission wavelengths for each system, and we note that the spectrum of the NR+PNW system was shifted by ≈ 2 nm relative to that of the NR alone. This spectral shift may be due to polymer-induced strain on the substrate from possible shrinkage of the cold DLW polymer.^[19,38] Nevertheless, the emission lines can be uniquely identified by the structure of the spectra over a wide bandwidth, as shown in the figure. The spectra in Figure 5d were taken near QD

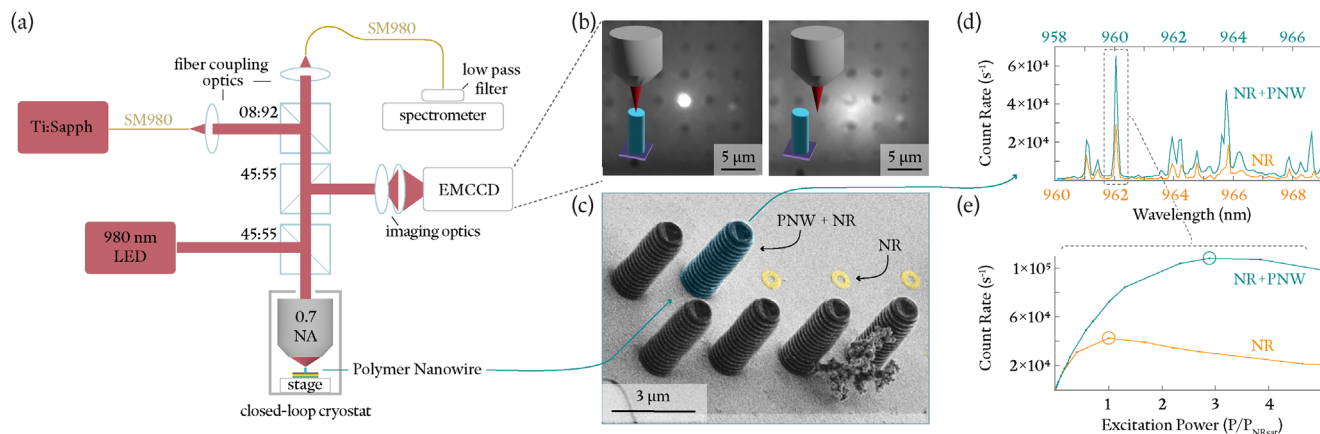


Figure 5. a) Schematic of the micro-photoluminescence setup used for PNW characterization (see main text for details). b) Images captured by the EMCCD camera when an excitation beam is aligned-to and confined by a PNW (left) and when the beam is laterally displaced from that PNW (right) showing beam divergence. Substrate illumination in this image is provided by an incoherent LED. A PNW array makes up the dark circles in the images. c) False color SEM image of nine NRs (yellow) with PNWs fabricated on top of six of the NR locations. Data from the highlighted NR+PNW is presented in panels (d,e) before and after PNW fabrication. d) Emission spectra collected from the test site indicated in panel (c) before (i.e., a NR only system) and after the fabrication of the PNW (i.e., a NR+PNW system), showing a broadband spectral enhancement of emission lines in the NR+PNW system over a span of 9 nm. Spectral shift discussed in main text. e) Power series for the highest intensity peak of the NR system (orange) and the NR+PNW system (green), showing a factor of $\approx 2.6\times$ enhancement at QD saturation. The spectra shown in (d) correspond to the circled data points in (e).

saturation, at powers indicated by the open circles in Figure 5e. We observe a broadband spectral enhancement of QD emission in the NR+PNW system compared to the NR system alone.

As a representative single-QD comparison, the emission of the spectral line at ≈ 962 nm was studied for increasing amounts of excitation power, as shown in Figure 5e in units of NR saturation power. At saturation, the maximum count rates measured at the spectrometer were ≈ 42000 s^{-1} for the NR system and ≈ 108000 s^{-1} for the NR+PNW. This observed enhancement factor of $2.6\times$ is inline with the $\approx 3.3\times$ enhancement predicted in Figure 1f for an SM980 (NA = 0.21) fiber-coupled input to the spectrometer. We note however, that the count rate enhancement is achieved at an excitation power $3\times$ greater than that of the NR device alone. The PNW was designed with a 1.4 μm diameter to prevent spurious reflections at the NR's surface during fabrication, at the cost of becoming a multi-mode waveguide for light at 950 nm, as shown in Figure 1h. Thus, the 780 nm excitation beam likely couples to an even greater number of modes, some of which may not excite the QD in the NR configuration with the same efficacy as the free-space beam in the NR configuration. In principle, the excitation efficiency can be optimized by using a PNW that is single mode at both the excitation and emission wavelengths, but in this study the minimum PNW diameter is restricted to avoid the NR reflections. On average, we observe a $(3.0 \pm 0.7)\times$ enhancement over the spectral window shown in Figure 5e, where the error represents the standard deviation of five prominent spectral lines and the leading source of error is likely the distribution of the underlying QDs near the principal axis of the PNW. In general, the PNW has enhanced the fiber-coupling of the NR platform by directly waveguide-coupling its emission to the HE_{11} optical mode, and we expect further improvements to be possible through the use of modified PNW designs (e.g., elliptical PNWs), modified NRs (e.g., optimized for PNW coupling), different underlying devices (e.g., circular Bragg gratings^[39–41]), or individually pre-positioned QDs.

3. Conclusion

We have demonstrated that DLW can be used to fabricate PNWs that directly waveguide-couple the emission from InAs/GaAs QDs while increasing collection efficiency into a down-stream fiber. Using numerical simulations, we show that dipole emission can be coupled to the optical modes within a PNW, which is expected to increase the collection efficiency by a down-stream single mode fiber due to the large overlap of a PNW's HE_{11} mode with the LP_{01} mode of a single mode fiber. We have also shown that PNWs are compatible with other on-chip devices like metallic NRs, since they do not require etching or modification of the underlying substrate. PNWs were fabricated on reflective substrates with DLW by suppressing standing wave reflections and mitigating heat generation. Comparing a NR system before and after the fabrication of a PNW, the maximum increase in the collection of the saturated flux of a single QD emission line when coupling the excitation light through the PNW is approximately threefold, with the variation between devices likely due to the uncontrolled spatial positions of the QDs with respect to the NR and PNW. Although recent studies have shown enhancements of approximately $2\text{--}8\times$ using DLW micro-optic lenses,^[14,19,38] different underlying devices in the micro-optic and PNW scenarios do not allow for a direct comparison. However, we note that the PNWs in this study achieve comparable results with drastically reduced device volumes and a different underlying collection mechanism. Our realization of wavelength-scale PNWs near the surface of a substrate that is both reflective and absorptive brings new functionality to the expanding field of 3D quantum photonic circuitry, and we expect that advances in DLW fabrication, PNW design, and modified on-chip devices will continue to improve the performance of PNW-enhanced systems.

This investigation has focused on azimuthally symmetric PNWs that are perpendicular to the device substrate, but a broadband PNW (or NR+PNW), like those in this study, also offers

full 3D flexibility. This may make PNWs well suited for use with other solid state devices, like micro-pillars and circular Bragg gratings. For example, the confined photons can be rerouted to other on-chip elements as in various examples of photonic wire-bonding.^[13] In particular, PNWs may be especially well suited for this function when used in conjunction with III-V nanowires,^[11] where the HE_{11} mode of the III-V nanowire can be well coupled to the HE_{11} mode of the PNW, which then routes the SP emission. We further note that the use of anti-reflection coatings (at the DLW lithography wavelength) on the surface of the GaAs may further improve PNW quality, as would the use of a distributed Bragg reflection mirror as the system's back reflector (at the cost of reduced reflection bandwidth). Finally, other possibilities include the use of elliptical nanowires for polarization-maintaining emission, or tapered PNWs that adiabatically transfer power from the higher order modes to the fundamental HE_{11} mode for further-improved performance.

Supporting Information

Supporting Information is available from the Wiley Online Library or from the author.

Acknowledgements

This work was supported by the NIST-on-a-chip program and the Leverhulme Trust, Grant IAF-2019-01. J.D.S. would like to acknowledge the partial support received from the IITP grant, which was funded by the Korean government (MSIT 2020-0-00841).

Conflict of Interest

The authors declare no conflict of interest.

Author Contributions

E. P. led the project, PNW design and fabrication, and conducted experiments. C.H. conducted optical characterization experiments, contributed to theoretical understanding and data analysis. M. D. contributed to theoretical understanding, the design of the PNWs, and the interpretation of data. J. D. S. grew the high density InAs/GaAs QDs. L. S. contributed to the theoretical understanding of PNWs, their design, and the fabrication of devices. K. S. contributed to the theoretical understanding of PNWs, standing wave mitigation, and data analysis. E. P. and K. S. prepared the manuscript. All authors contributed and discussed the content of this manuscript.

Data Availability Statement

The data that support the findings of this study are available from the corresponding author upon reasonable request.

Keywords

direct laser writing, epitaxial quantum dots, nanophotonics, single photon sources

Received: May 26, 2023
Revised: September 18, 2023
Published online:

- [1] N. Sangouard, H. Zbinden, *J. Mod. Opt.* **2012**, *59*, 1458.
- [2] T. E. Northup, R. Blatt, *Nat. Photonics* **2014**, *8*, 356.
- [3] I. Aharonovich, D. Englund, M. Toth, *Nat. Photonics* **2016**, *10*, 631.
- [4] F. Flamini, N. Spagnolo, F. Sciarrino, *Rep. Prog. Phys.* **2018**, *82*, 016001.
- [5] N. Tomm, A. Javadi, N. O. Antoniadis, D. Najer, M. C. Löbl, A. R. Korsch, R. Schott, S. R. Valentin, A. D. Wieck, A. Ludwig, R. J. Warburton, *Nat. Nanotechnol.* **2021**, *16*, 399.
- [6] H. Wang, Y.-M. He, T.-H. Chung, H. Hu, Y. Yu, S. Chen, X. Ding, M.-C. Chen, J. Qin, X. Yang, R.-Z. Liu, Z.-C. Duan, J.-P. Li, S. Gerhardt, K. Winkler, J. Jurkat, L.-J. Wang, N. Gregersen, Y.-H. Huo, Q. Dai, S. Yu, S. Höfling, C.-Y. Lu, J.-W. Pan, *Nat. Photonics* **2019**, *13*, 770.
- [7] P. Senellart, G. Solomon, A. White, *Nat. Nanotechnol.* **2017**, *12*, 1026.
- [8] L. Zhai, G. N. Nguyen, C. Spinnler, J. Ritzmann, M. C. Löbl, A. D. Wieck, A. Ludwig, A. Javadi, R. J. Warburton, *Nat. Nanotechnol.* **2022**, *17*, 829.
- [9] L. Bremer, C. Jimenez, S. Thiele, K. Weber, T. Huber, S. Rodt, A. Herkommer, S. Burger, S. Höfling, H. Giessen, S. Reitzenstein, *Opt. Express* **2022**, *30*, 15913.
- [10] N. Tomm, A. Javadi, N. O. Antoniadis, D. Najer, M. C. Löbl, A. R. Korsch, R. Schott, S. R. Valentin, A. D. Wieck, A. Ludwig, R. J. Warburton, *Nat. Nanotechnol.* **2021**, *16*, 399.
- [11] H. Mäntynen, N. Anttu, Z. Sun, H. Lipsanen, *Nanophotonics* **2019**, *8*, 747.
- [12] P.-I. Dietrich, M. Blaicher, I. Reuter, M. Billah, T. Hoose, A. Hofmann, C. Caer, R. Dangel, B. Offrein, U. Troppenz, M. Moehrl, W. Freude, C. Koos, *Nat. Photonics* **2018**, *12*, 241.
- [13] N. Lindenmann, G. Balthasar, D. Hillerkuss, R. Schmogrow, M. Jordan, J. Leuthold, W. Freude, C. Koos, *Opt. Express* **2012**, *20*, 17667.
- [14] M. Sartison, K. Weber, S. Thiele, L. Bremer, S. Fischbach, T. Herzog, S. Kolatschek, M. Jetter, S. Reitzenstein, A. Herkommer, P. Michler, S. L. Portalupi, H. Giessen, *Light Adv. Manuf.* **2021**, *2*, 103.
- [15] E. Perez, G. Moille, X. Lu, D. Westly, K. Srinivasan, *Opt. Express* **2020**, *28*, 39340.
- [16] R. M. R. Adão, T. L. Alves, C. Maibohm, B. Romeira, J. B. Nieder, *Opt. Express* **2022**, *30*, 9623.
- [17] J. Moughames, X. Porte, M. Thiel, G. Ulliac, L. Larger, M. Jacquot, M. Kadic, D. Brunner, *Optica* **2020**, *7*, 640.
- [18] S. Fischbach, A. Schlehahn, A. Thoma, N. Srocka, T. Gissibl, S. Ristok, S. Thiele, A. Kaganskiy, A. Strittmatter, T. Heindel, S. Rodt, A. Herkommer, H. Giessen, S. Reitzenstein, *ACS Photonics* **2017**, *4*, 1327.
- [19] L. Bremer, K. Weber, S. Fischbach, S. Thiele, M. Schmidt, A. Kaganskiy, S. Rodt, A. Herkommer, M. Sartison, S. L. Portalupi, P. Michler, H. Giessen, S. Reitzenstein, *APL Photonics* **2020**, *5*, 106101.
- [20] L. Bremer, S. Rodt, S. Reitzenstein, *Mater. Quantum Technol.* **2022**, *2*, 042002.
- [21] A. W. Schell, J. Kaschke, J. Fischer, R. Henze, J. Wolters, M. Wegener, O. Benson, *Sci. Rep.* **2013**, *3*, 1577.
- [22] M. Colautti, P. Lombardi, M. Trapuzzano, F. S. Piccioli, S. Pazzagli, B. Tiribilli, S. Nocentini, F. S. Cataliotti, D. S. Wiersma, C. Toninelli, *Adv. Quantum Technol.* **2020**, *3*, 2000004.
- [23] J. Liu, K. Konthasinghe, M. Davanço, J. Lawall, V. Anant, V. Verma, R. Mirin, S. W. Nam, J. D. Song, B. Ma, Z. S. Chen, H. Q. Ni, Z. C. Niu, K. Srinivasan, *Phys. Rev. Appl.* **2018**, *9*, 064019.
- [24] C. Haws, E. Perez, M. Davanco, J. D. Song, K. Srinivasan, L. Sapienza, *Appl. Phys. Lett.* **2022**, *120*, 081103.
- [25] O. J. Trojak, S. I. Park, J. D. Song, L. Sapienza, *Appl. Phys. Lett.* **2017**, *111*, 021109.
- [26] C. Haws, B. Guha, E. Perez, M. Davanco, J. D. Song, K. Srinivasan, L. Sapienza, *Mater. Quantum Technol.* **2022**, *2*, 025003.

- [27] M. Schmid, D. Ludescher, H. Giessen, *Opt. Mater. Express* **2019**, *9*, 4564.
- [28] H. Huang, S. Manna, C. Schimpf, M. Reindl, X. Yuan, Y. Zhang, S. F. C. da Silva, A. Rastelli, *Adv. Opt. Mater.* **2021**, *9*, 2001490.
- [29] S. Fischbach, A. Kaganskiy, E. B. Y. Tauscher, F. Gericke, A. Thoma, R. Schmidt, A. Strittmatter, T. Heindel, S. Rodt, S. Reitzenstein, *Appl. Phys. Lett.* **2017**, *111*, 011106.
- [30] O. J. Trojak, C. Woodhead, S.-I. Park, J. D. Song, R. J. Young, L. Sapienza, *Appl. Phys. Lett.* **2018**, *112*, 221102.
- [31] Certain commercial products or names are identified to foster understanding. Such identification does not constitute recommendation or endorsement by the National Institute of Standards and Technology, nor is it intended to imply that the products or names identified are necessarily the best available for the purpose.
- [32] T. Zandrini, N. Liaros, L. J. Jiang, Y. F. Lu, J. T. Fourkas, R. Osellame, T. Baldacchini, *Opt. Mater. Express* **2019**, *9*, 2601.
- [33] H.-B. Sun, S. Kawata, *J. Lightwave Technol.* **2003**, *21*, 624.
- [34] J. Purto, P. Rogin, A. Verch, V. E. Johansen, R. Hensel, *Nanomaterials* **2019**, *9*, 1495.
- [35] S. K. Saha, C. Divin, J. A. Cuadra, R. M. Panas, *J. Micro Nano-Manuf.* **2017**, *5*, 031002.
- [36] J. Purto, A. Verch, P. Rogin, R. Hensel, *Microelectron. Eng.* **2018**, *194*, 45.
- [37] E. M. Harnisch, T. Venek, S. Nohr, N. König, R. Schmitt, *Opt. Mater. Express* **2019**, *9*, 269.
- [38] M. Sartison, S. L. Portalupi, T. Gissibl, M. Jetter, H. Giessen, P. Michler, *Sci. Rep.* **2017**, *7*, 39916.
- [39] M. Davanço, M. T. Rakher, D. Schuh, A. Badolato, K. Srinivasan, *Appl. Phys. Lett.* **2011**, *99*, 041102.
- [40] J. Liu, R. Su, Y. Wei, B. Yao, S. F. C. da Silva, Y. Yu, J. Iles-Smith, K. Srinivasan, A. Rastelli, J. Li, X. Wang, *Nat. Nanotechnol.* **2019**, *14*, 586.
- [41] L. Sapienza, M. Davanço, A. Badolato, K. Srinivasan, *Nat. Commun.* **2015**, *6*, 7833.